

## Supporting Information

### **Ferromagnetic Co<sub>20</sub>Ni<sub>80</sub> nanoparticles encapsulated inside reduced graphene oxide layers with superior microwave absorption performance**

Xuefeng Yu<sup>a</sup>, Lei Wang<sup>a</sup>, Jiwei Liu<sup>b</sup>, Shuyan Xue<sup>a</sup>, Liting Yang<sup>a</sup>, Xiao Li<sup>a</sup>, Jie Zhang<sup>a</sup>, Linshen Xing<sup>a</sup>, Guanyu Chen<sup>a</sup>, Min Wang<sup>\*a</sup> and Renchao Che<sup>\*a</sup>

<sup>a</sup>Laboratory of Advanced Materials, Department of Materials Science and Collaborative Innovation Center of Chemistry for Energy Materials (iChem), Fudan University, Shanghai 200438, P. R. China

<sup>b</sup>School of Materials Science and Engineering, Changzhou University, Changzhou, Jiangsu 213164, People's Republic of China

\* E-mail: [rcche@fudan.edu.cn](mailto:rcche@fudan.edu.cn)

\* E-mail: [minwang@fudan.edu.cn](mailto:minwang@fudan.edu.cn)

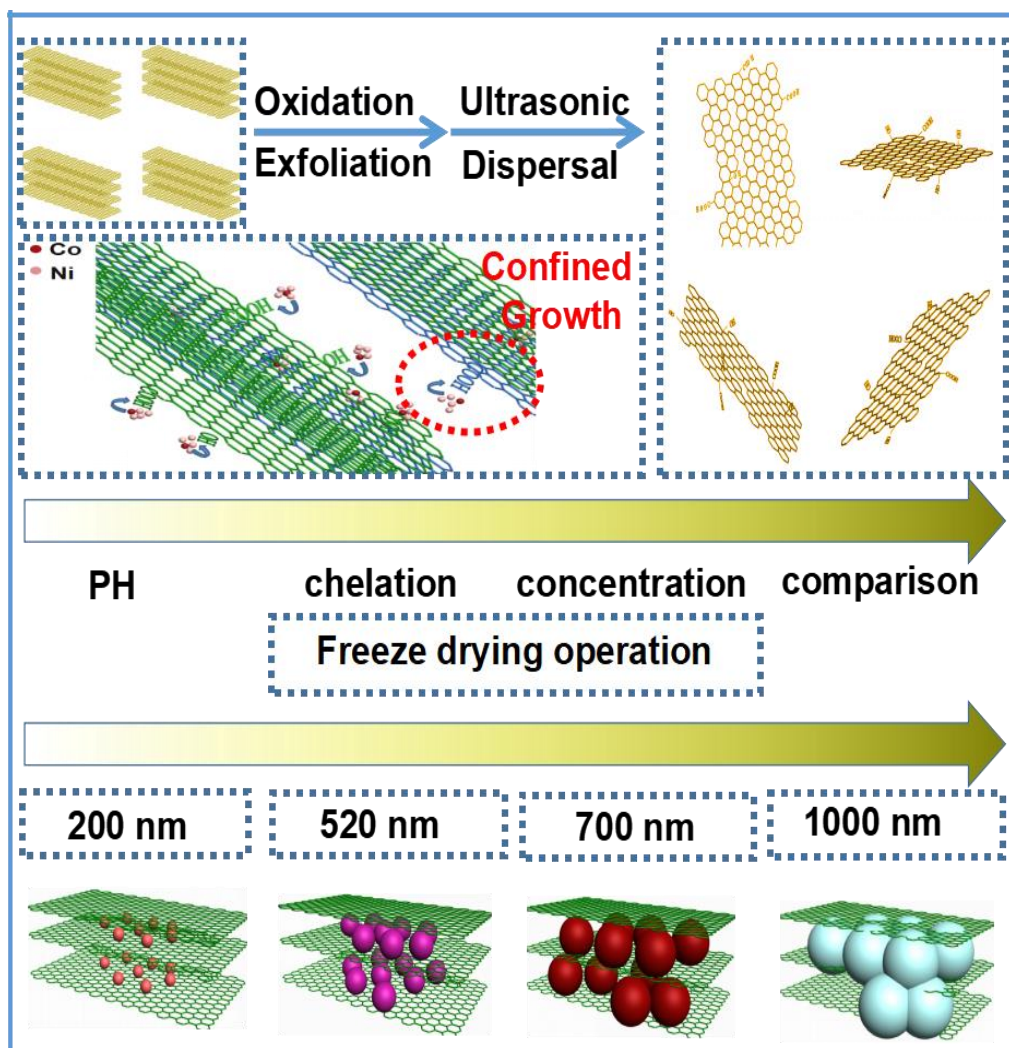


Fig S1. The syntheses schematics for rGO/Co<sub>20</sub>Ni<sub>80-1</sub>, rGO/Co<sub>20</sub>Ni<sub>80-2</sub>, rGO/Co<sub>20</sub>Ni<sub>80-3</sub> and rGO/Co<sub>20</sub>Ni<sub>80-4</sub> nanocomposites

Fig S1<sup>†</sup> illustrates the synthetic routes of the series of rGO/Co<sub>20</sub>Ni<sub>80-x</sub> nanocomposites in details exhibiting several key factors for adjusting the nanoparticle sizes. GO sheets were prepared by the oxidation and a followed exfoliation of Graphite flakes, which possess abundant oxygen groups (COO<sup>-</sup> or OH<sup>-</sup>). Because of the richly negative charges, these groups actively function as the confined-growth sites to capture cobalt and nickel ions (Co<sup>2+</sup>:Ni<sup>2+</sup> =1:4) and form C–O–Ni or C–O–Co linkages in the hydrothermal reaction.<sup>1</sup> These attracted ions crystallize, grow and

chelate uniformly on the surface of GO layer. Meanwhile, the GO layer was also reduced, which hindered the aggregation of  $\text{Co}_{20}\text{Ni}_{80}$  nanocrystals and further promoted their formation. On the other hand, the physicochemical properties of precursor solution have a significant effect on nanoparticle morphology (shape, size). Marked by yellow arrows, the four different nanoparticle sizes could be tailored by the solution pH, chelating agent species, and precursor concentration. In terms of pH, citric acid is added instead of sodium hydroxide with same mass. Due to the acidic environment, the lower pressure atmosphere is formed which results in a weaker driving force for grain growth. Furthermore, the excessive citric acid facilitates the dispersion of metal ions, which also contributed to the reduction in nanoparticle size. Using half volume of DEG to replace EG, the solvent nature is changed and the superior chelating of DEG may be more detrimental effects for nanoparticle growth kinetics. Moreover, if the more precursor concentration are added, the more crystallization opportunity could form. Thereby, the specified nanoparticle sizes that correspond to different hydrothermal conditions could be obtained. They are respectively 200 nm for rGO/ $\text{Co}_{20}\text{Ni}_{80}$ -1, 520 nm for rGO/ $\text{Co}_{20}\text{Ni}_{80}$ -2, 700 nm for rGO/ $\text{Co}_{20}\text{Ni}_{80}$ -3 and 1100 nm for rGO/ $\text{Co}_{20}\text{Ni}_{80}$ -4. Finally, the 3D framework structure of rGO/ $\text{Co}_{20}\text{Ni}_{80}$  nanocomposites as sandwich-like could be got through a freeze drying process. The similar structure is also agreed with the reported

literature.<sup>2,3</sup>

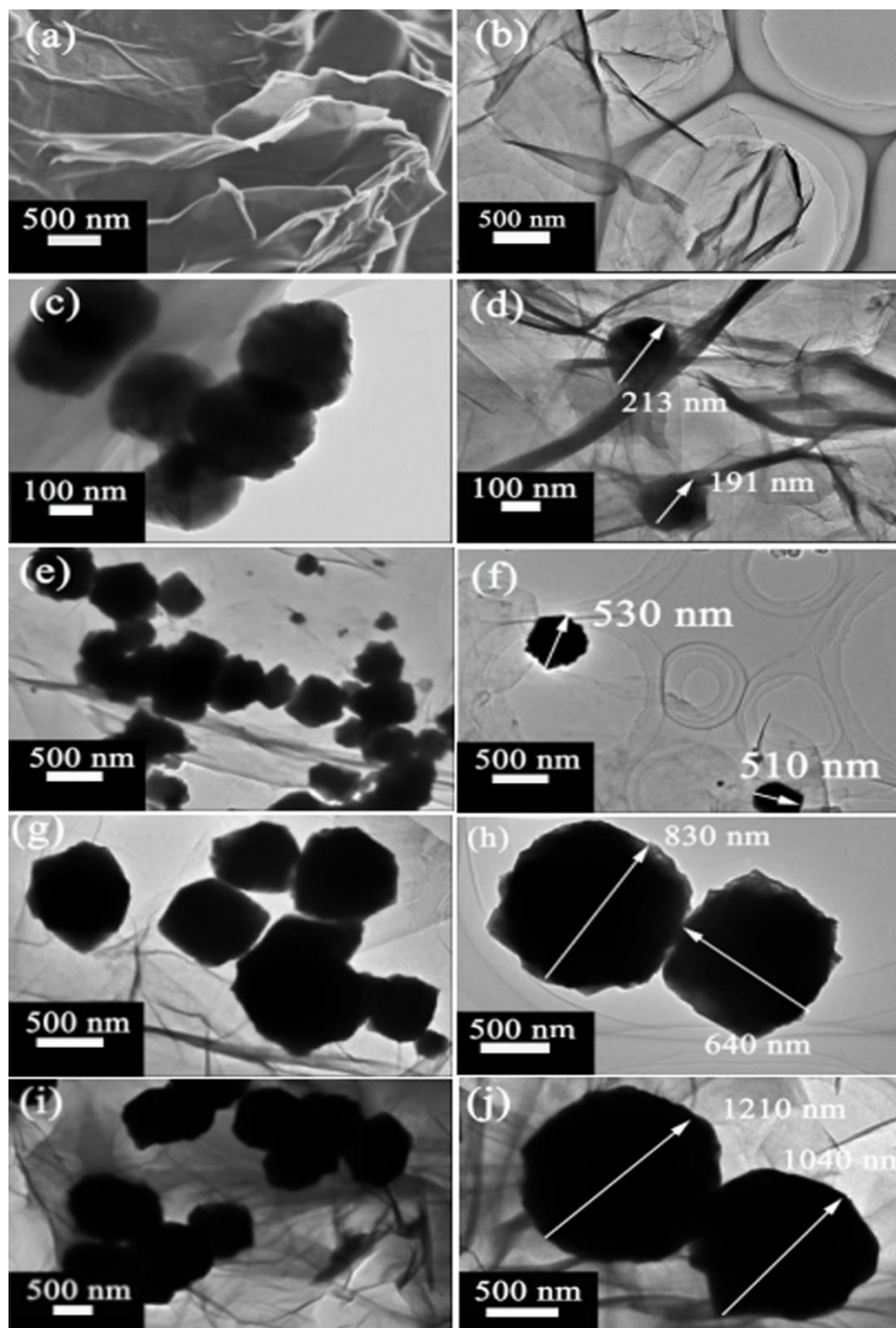


Fig S2. TEM images (a)-(b) of GO and (c)-(j) of rGO/Co<sub>20</sub>Ni<sub>80-x</sub> nanocomposites with different nanoparticle sizes: (c)-(d) rGO/Co<sub>20</sub>Ni<sub>80-1</sub>; (e)-(f) rGO/Co<sub>20</sub>Ni<sub>80-2</sub>; (g)-(h) rGO/Co<sub>20</sub>Ni<sub>80-3</sub>; (i)-(j) rGO/Co<sub>20</sub>Ni<sub>80-4</sub>.

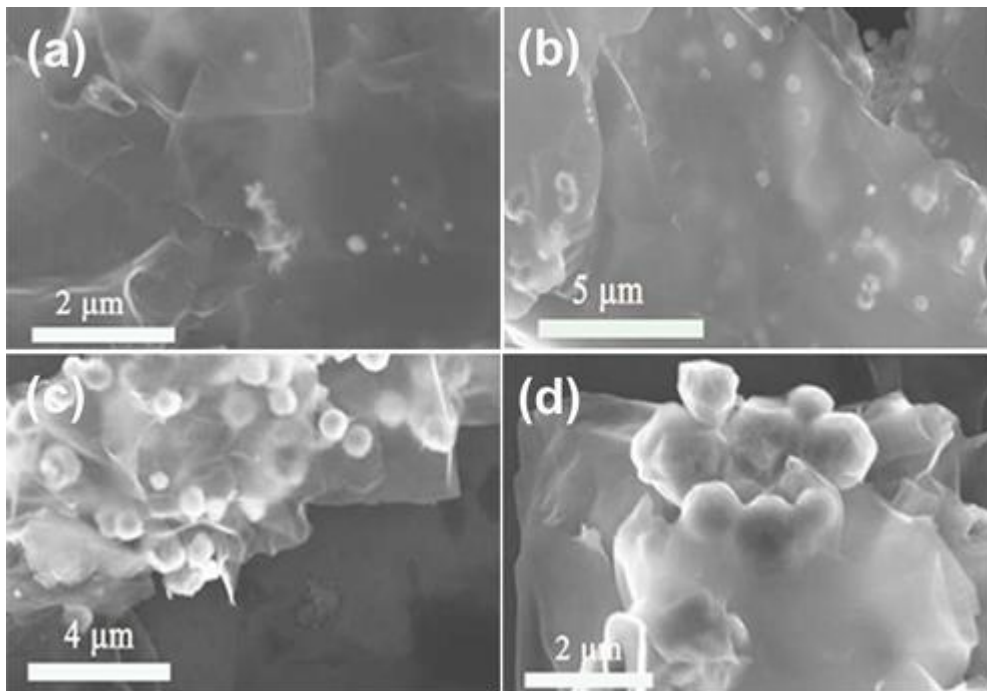


Fig S3. The SEM images (a)-(d) of  $rGO/Co_{20}Ni_{80-x}$  nanocomposites : (a)  $rGO/Co_{20}Ni_{80-1}$ ; (b)  $rGO/Co_{20}Ni_{80-2}$ ; (c)  $rGO/Co_{20}Ni_{80-3}$ ; (d)  $rGO/Co_{20}Ni_{80-4}$ .

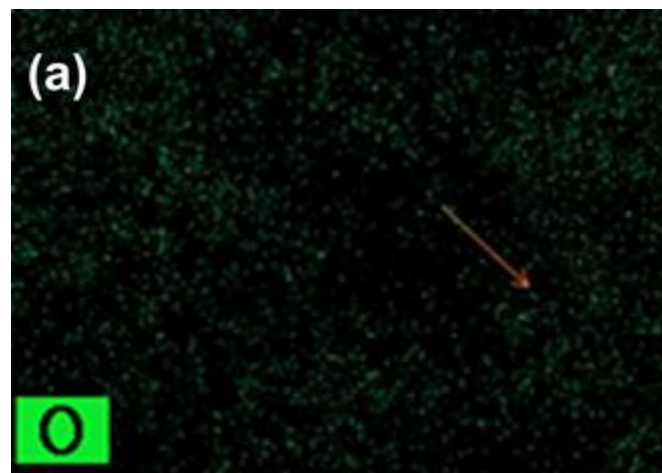


Fig S4. The mapping image of O element of  $rGO/Co_{20}Ni_{80-2}$  nanocomposite.

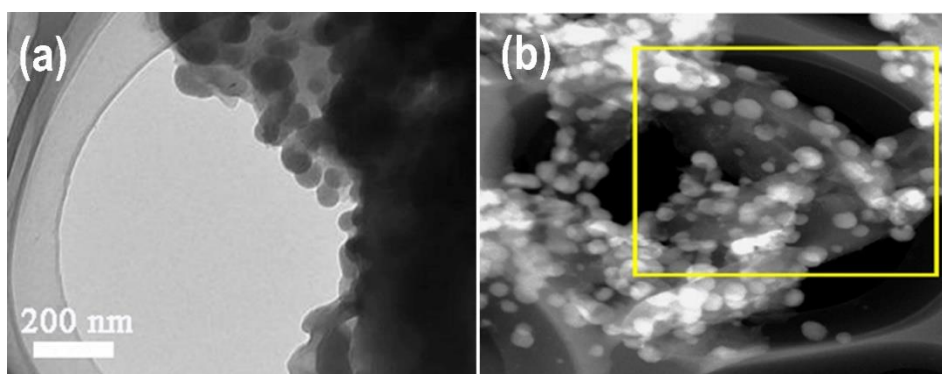


Fig S5. The TEM image (a) of shattered rGO/Co<sub>20</sub>Ni<sub>80-2</sub> nanocomposite by slicing technology. (b) HADFF-STEM image of shattered rGO/Co<sub>20</sub>Ni<sub>80-2</sub> nanocomposite.

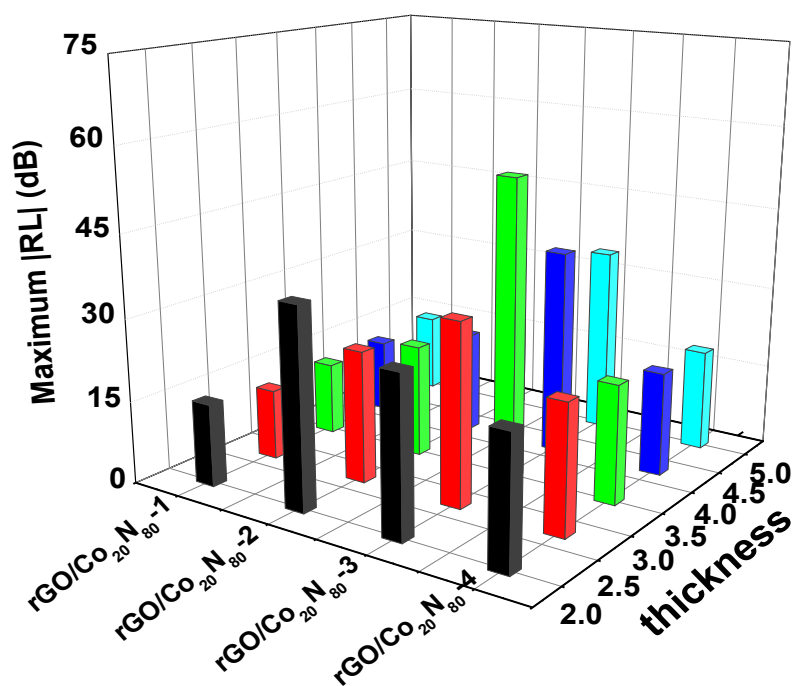


Fig S6. The comparison of the maximum |RL| of rGO/Co<sub>20</sub>Ni<sub>80-x</sub> nanocomposites with a same absorber thickness in the frequency range of 2-18 GHz.

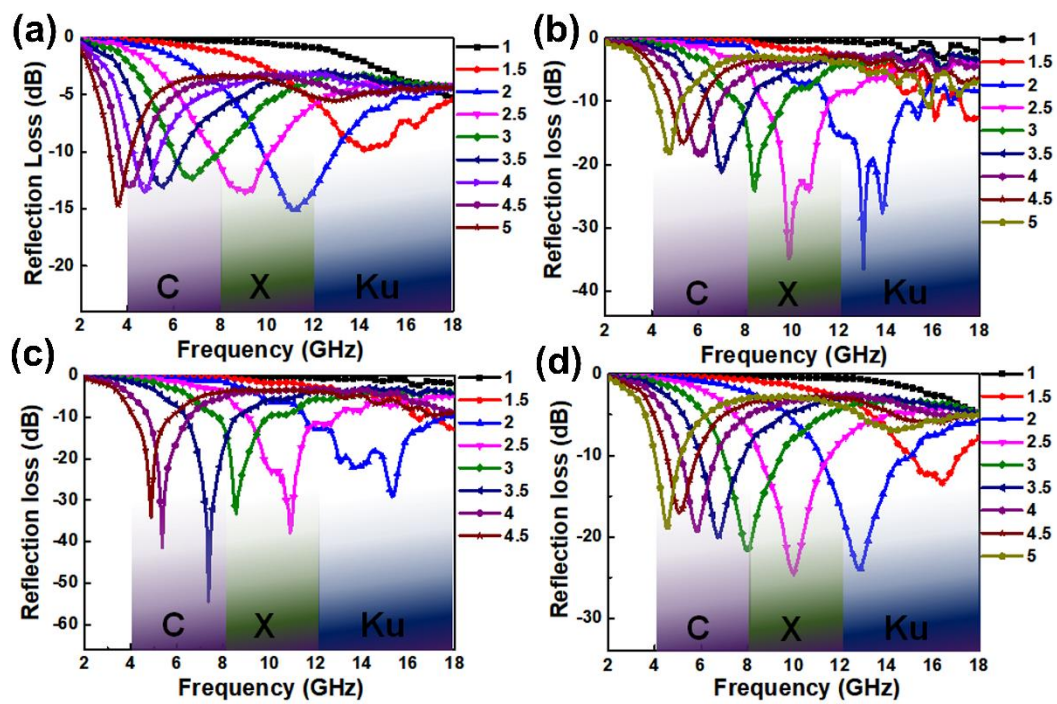


Fig S7. The full-band microwave reflection losses of (a) rGO/Co<sub>20</sub>Ni<sub>80</sub>-1; (b) rGO/Co<sub>20</sub>Ni<sub>80</sub>-2; (c) rGO/Co<sub>20</sub>Ni<sub>80</sub>-3, and (d) rGO/Co<sub>20</sub>Ni<sub>80</sub>-4 nanocomposites with different thicknesses in the frequency range of 2-18 GHz.

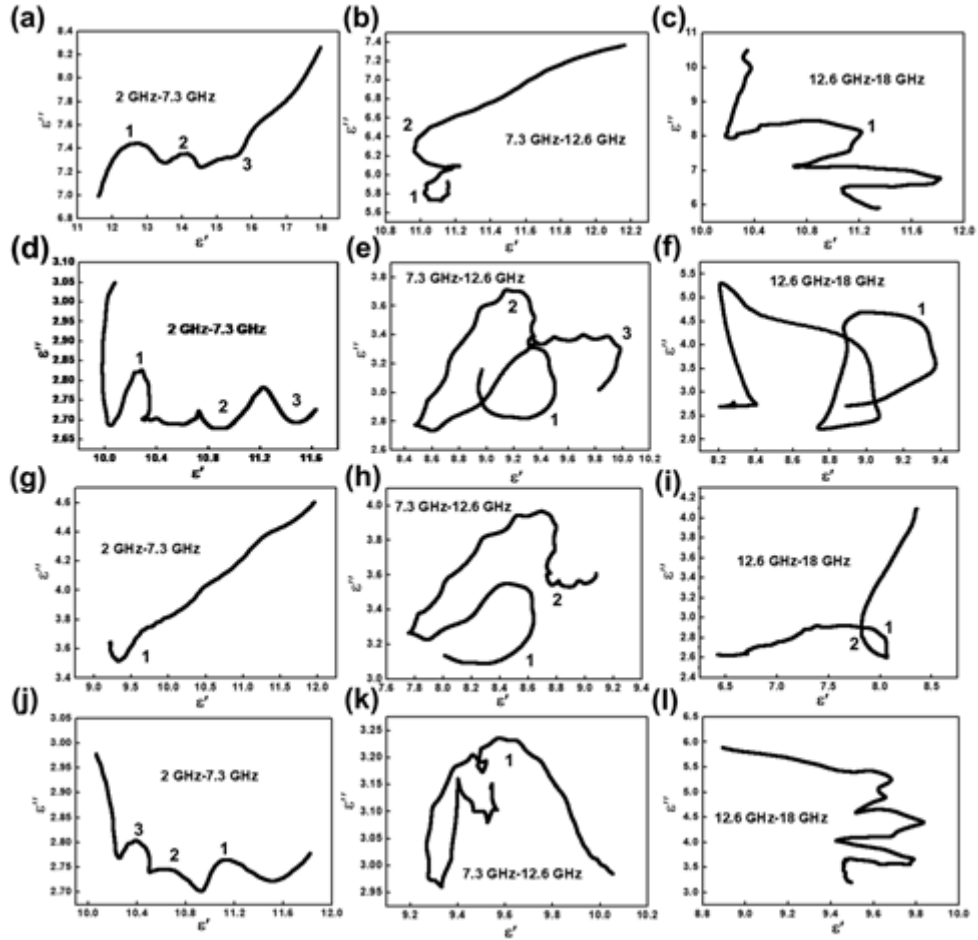


Fig S8. The typical Cole-Cole semicircles ( $\epsilon''$  vs  $\epsilon'$ ) of rGO/Co<sub>20</sub>Ni<sub>80-x</sub> nanocomposites in different three frequency region. (a)-(c): rGO/Co<sub>20</sub>Ni<sub>80-1</sub>; (d)-(f): rGO/Co<sub>20</sub>Ni<sub>80-2</sub>; (g)-(i): rGO/Co<sub>20</sub>Ni<sub>80-3</sub>; (j)-(l): rGO/Co<sub>20</sub>Ni<sub>80-4</sub>.

Generally, the Debye relaxation process could be described by the Cole-Cole semicircle. As followed, the relative complex permittivity  $\epsilon_r$  is calculated according to Debye relaxation theory<sup>4</sup>

$$\epsilon_r = \epsilon_\infty + \frac{\epsilon_s - \epsilon_\infty}{1 + j2\pi f\tau} = \epsilon' - j\epsilon'' \quad (1)$$

in which  $f$  is the frequency,  $\tau$  is the polarization relaxation time,  $\epsilon_s$  and  $\epsilon_\infty$  are respectively the stationary permittivity and optical dielectric constant at the high-frequency limit. Moreover, it can be further deduced that:



$$\varepsilon' = \varepsilon_{\infty} + \frac{\varepsilon_s - \varepsilon_{\infty}}{1 + (2\pi f)^2 \tau^2} \quad (2)$$

$$\varepsilon'' = \frac{2\pi f \tau (\varepsilon_s - \varepsilon_{\infty})}{1 + (2\pi f)^2 \tau^2} \quad (3)$$

According to eqn (2) and (3), the relationship between  $\varepsilon'$  and  $\varepsilon''$  can be expressed as:

$$(\varepsilon' - \varepsilon_{\infty})^2 + (\varepsilon'')^2 = (\varepsilon_s - \varepsilon_{\infty})^2 \quad (4)$$

Based on eqn (4), the conclusion is clear that a curve of  $\varepsilon'$  versus  $\varepsilon''$  could exhibit a single semicircle. Each semicircle existence indicates one Debye relaxation occurring.

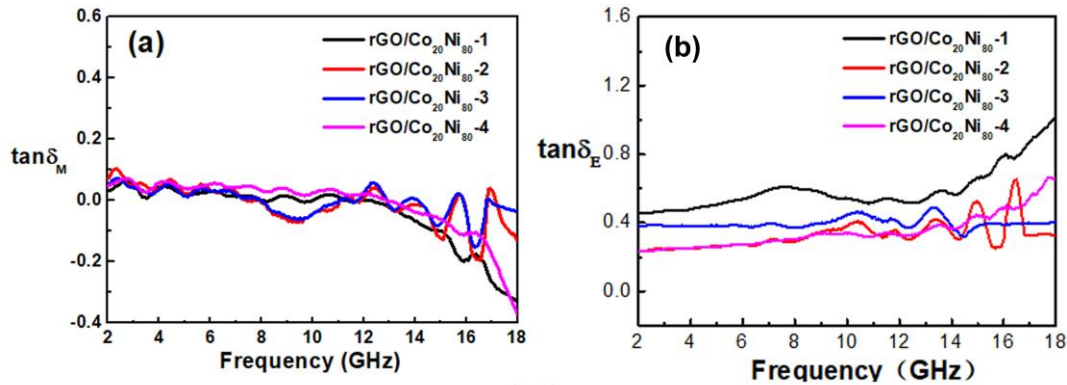


Fig S9. The dielectric loss tangent (a) and magnetic loss tangent (b) of rGO/Co<sub>20</sub>Ni<sub>80-x</sub> nanocomposites in the frequency range of 2-18 GHz. They represent dielectric loss ability (a) and magnetic loss ability (b).

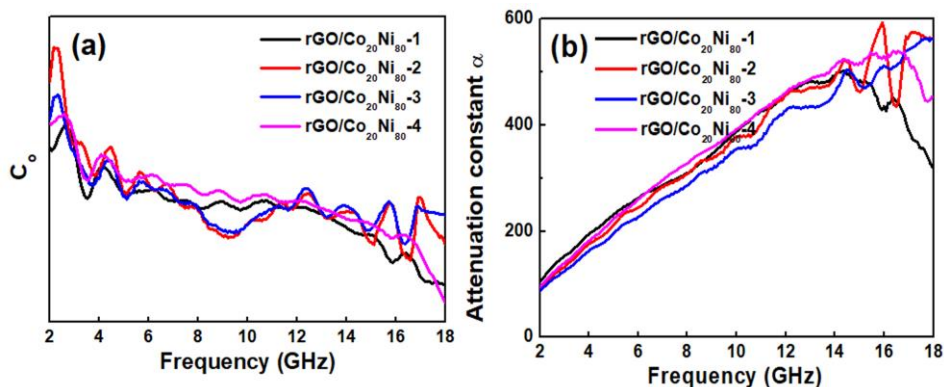


Fig S10.  $C_o$  values (a) of rGO/Co<sub>20</sub>Ni<sub>80-x</sub> nanocomposites; attenuation constant  $\alpha$  (b) of rGO/Co<sub>20</sub>Ni<sub>80-x</sub> nanocomposites in the frequency range of 2-18 GHz.

Table S3. The quantitative analysis of rGO/Co<sub>20</sub>Ni<sub>80-2</sub> nanocomposite implemented by EDS. The signal of silicon element (Si) mainly comes from Si-substrate.

Elements	Atomic number	Mass (%)	Normalized mass (%)	Atomic (%)	Abs.error (%) (1 sigma)	Rel.error (%) (1 sigma)
C	6	57.90	57.76	80.80	6.66	11.51
O	8	5.82	5.80	6.10	0.88	15.06
Co	27	5.24	5.23	1.49	0.20	3.78
Ni	28	22.68	22.62	6.48	0.74	3.25
Si	14	8.60	8.58	5.14	0.39	4.49
	Total:	100.24	100.00	100.00		

## Reference

1. Y. Zhang, X. Wang and M. Cao, *Nano Research*, 2018, **11**, 1426-1436.
2. X. J. Zhang, G. S. Wang, W. Q. Cao, Y. Z. Wei, J. F. Liang, L. Guo and M. S. Cao, *ACS applied materials & interfaces*, 2014, **6**, 7471-7478.

3. C. Hu, Z. Mou, G. Lu, N. Chen, Z. Dong, M. Hu and L. Qu, *Physical chemistry chemical physics : PCCP*, 2013, **15**, 13038-13043.
4. Y. Du, W. Liu, R. Qiang, Y. Wang, X. Han, J. Ma and P. Xu, *ACS applied materials & interfaces*, 2014, **6**, 12997-13006.